# Ablation and surface structuring of Si₃N₄ ceramics by nanosecond laser pulses

N. Nedyalkov[1] · A. Dikovska[1] · K. Grochowska[2] · R. Jendrzejewski[2] · L. Aleksandrov[3] · T. Dilova[3] · G. Atanasova[3]

## Abstract

The work presents the main characteristics of the process of ablating silicon nitride ceramics by nanosecond laser pulses. Two types of ceramics are considered—tape cast and gas pressure sintered. Laser processing was performed by a Q-switched Nd:YAG laser system at four wavelengths—266 nm, 355 nm, 532 nm, and 1064 nm. The ablation depth dependences on the laser fluence and number of pulses applied at the different wavelengths are presented and discussed. It is found that increasing the laser fluence at a fixed number of pulses leads to a saturation of the ablation depth for all wavelengths used. Further, laser treatment results in a variety of micro- and nanostructures on the surface of the material. Their characteristics are determined as a function of the processing parameters. The ablation process proceeds via decomposition of the ceramic, as traces of silicon and silicon oxide are found in the processed area. The dependences observed are discussed based on a detailed analysis of the morphological and chemical changes estimated by classical analytical methods, namely, SEM, TEM, XRD, XPS, and Raman spectroscopy. The study presented can serve as a basis for the development of a laser-based processing technique for nitride ceramics and fabrication of Si-based composites.

**Keywords** Laser processing · Surface structuring · Silicon nitride ceramics · Nitride ceramics decomposition

## 1 Introduction

Nitride ceramics are sintered materials with properties suitable for uses in a number of modern applications [1]. They are hard, wear, and corrosion-resistant materials and exhibit high-temperature stability, good insulator properties, and high heat conductivity [2, 3]. Based on these, efficient applications of these materials have been well established as machine tools in materials processing and in high-power electronics [4]. Silicon nitride is a typical representative of this class of ceramic materials and has attracted interest from the viewpoint of efficient applications in different industries,

but also from the fundamental aspects of understanding, developing, and optimizing technologies of fabricating artificial materials and manipulating their properties [5]. Being a ceramic material, it possesses a low thermal expansion coefficient that reflects on its high thermal shock resistance; it is also chemically inert to many molten metals and has a high temperature stability up to about 1800 °C [2]. The Si₃N₄ ceramic also shows a high wear resistance and a high strength. The material is of low density and can be efficiently used in medicine as material for implants [6, 7], in moving parts in motors [8, 9] and in the airplane industry [10]. The wide range of demonstrated applications also includes the fabrication of casting nozzles and of high-temperature components in complex systems in metallurgy, as cutting tools for steel, of protective covers of fibers, and of Si components in electronics and solar cells [2, 5, 10]. One of the main problems related to using the Si₃N₄ ceramic arises from its fracture behavior—if cracks are formed into the material, they may rapidly propagate within a large volume leading to destruction of the components [4]. This characteristic influences this ceramic efficiency of application, but it is also an issue when processing the material, e.g., when drilling and cutting is considered. The solution of this problem

✉ N. Nedyalkov
 nned@ie.bas.bg

1 Institute of Electronics, Bulgarian Academy of Sciences, 72, Tsarigradsko Chaussee Blvd., 1784 Sofia, Bulgaria

2 The Szewalski Institute of Fluid-Flow Machinery, Polish Academy of Sciences, 14 Fiszera Str., 80-231 Gdańsk, Poland

3 Institute of General and Inorganic Chemistry, Bulgarian Academy of Sciences, Bld. 11, Acad. Georgi Bonchev Str., 1113 Sofia, Bulgaria

is assumed to lie in the sintering recipe, which may influence the material's microstructure and, consequently, its mechanical properties. At present, silicon nitride ceramic is fabricated by several main approaches—hot pressure, gas pressure, pressure-less synthesis, and tape cast sintering [11–13], as the different formation mechanisms result in differences in the material's properties. A solution for achieving high-efficiency and high-quality silicon nitride ceramic processing is also sought in view of application of different treatment techniques [4]. As an approach alternative to the mechanical methods, the use of lasers has demonstrated promising benefits [14–17]. The main feature of the process is the improved material's plasticity after undergoing laser heating, which improves the machinability and quality of the surface finish. The non-mechanical contact method of interaction and the availability of laser systems operating within a wide range of parameters would offer precise and efficient machining, with the affected zone being reduced to a few micrometers only. It has also been demonstrated that multiple laser passes could reduce the thermal stresses and cracking of the $Si_3N_4$ ceramic [18]. The research performed so far has clearly indicated that the mechanisms responsible for material removal are related to oxidation, melting and vaporization, but their impact strongly depends on the processing conditions. It should also be mentioned that laser processing may also offer surface structuring of the ceramic that may be crucial in some applications, as in tribology and biomedicine; however, it is yet to be widely regarded as a processing technique. The studies presented in the literature have been mainly devoted to using IR laser irradiation, rarely have other wavelengths been considered [19]. There is still a lack of research on the effects of different laser parameters, such as the wavelength used, on the laser ablation characteristics and the surface morphology produced. In addition, when results have been presented on laser processing of $Si_3N_4$ ceramics, no discussions have been devoted to the effect of the specific technology of fabricating the $Si_3N_4$ ceramics.

In this work, results are presented and compared on the main aspects of the ablation process of two types of $Si_3N_4$ ceramics. Gas pressure sintering is commonly used for bulk machine parts and tools for material processing. The second type is the type cast where the resulting material is a thin sheet. For this type, mechanical processing is a challenge, as it could be accompanied by crack formation and fracture of the material. Since the different fabrication techniques define differences in the material structure and composition, it is worth studying their response to laser processing. The latter itself includes complex phenomena where difference in the initial structure and composition may be crucial. Ablation characteristics—the ablation depth as a function of the laser fluence and number of pulses applied and the changes in the surface morphology and composition, are presented for

processing at different laser radiation wavelengths ranging from the UV to IR. Such comparative study for different types of $Si_3N_4$ ceramics at a wide range of laser wavelengths is not presented so far. The results provide detailed and novel data on the nanosecond ablation of silicon nitride ceramics and can be applied to the development of a laser-based technology for $Si_3N_4$ ceramic processing and surface structuring.

## 2 Experimental

The experiments on laser processing were performed using two types of $Si_3N_4$ ceramics—tape cast (TC) (CeramTec) and gas pressure sintered (GP) (Unipretec). The first type is used for efficient fabrication of ceramic sheets; the second one is widely used for fabrication of materials of complex shape. The TC type has a light gray color, while the GP $Si_3N_4$ is black. A typical TC-type sample has a thickness of about 0.3 mm that allows measuring the transmission spectra in the UV–IR spectral range, which in this work was conducted by using an Ocean Optics spectrometer with a 200–2000 nm light source. The thicknesses of the GP samples were about 2 mm. They were irradiated by the fundamental wavelength (1064 nm), the second (532 nm), the third (355 nm) and the fourth (266 nm) harmonics of a nanosecond Nd:YAG laser system (Lotis). The laser pulse duration was 15 ns and a repetition rate of 10 Hz was used. The laser radiation was focused by a quartz lens with a focal distance of 300 mm. For all wavelengths, the spot size on the ceramic surface was adjusted to about 500 μm. The experiments were carried out in air, and the dependences were obtained of the ablation depth and the surface morphology on the laser fluence and the number of pulses applied. The ablation depth were measured by an optical microscope (OPTIKA B-150); the correctness of the measurements was confirmed by a comparison with a cross-sectional image made by scanning electron microscopy (SEM, Hitachi TM 4000). The errors in the measured value are presented as standard deviation calculated from three measurements. The SEM system was also used for analysis of the surface morphology induced by laser radiation. The changes in the chemical composition due to the ablation process were analyzed based on TEM (JEOL JEM 2100) and Raman spectroscopy (micro-Raman, Renishaw In-via, 514 nm, laser spot size of 2 μm) observations. In the case of TEM, the sample was prepared as part of the material formed in the irradiated area was removed by a diamond tip and transferred to a TEM copper grid by a water droplet. XRD (Bruker D8 Advance diffractometer, CuKα radiation) was also employed to estimate the phase changes. XPS analysis of the surface composition was performed by means of an AXIS Supra electron spectrometer (Kratos Analytical Ltd.). The convolution analysis was carried out using the commercial data-processing software (ESCApe™ Kratos

Analytical Ltd.) considering a Shirley-type background and Gaussian–Lorentzian curve fitting.

# 3 Results and discussion

The ablation depth dependences on the laser fluence applied at the different wavelengths and the two type of ceramics, TC $Si_3N_4$ and GP $Si_3N_4$, are given in Fig. 1a and b, respectively. The number of pulses in all cases is 100. A general feature observed in all dependences is that in the fluence range up to few J/cm$^2$, the ablation depth increases rapidly with the fluence with an average rate (ablation depth per fluence) of about 10 μm/(J/cm$^2$). A second regime is established at higher fluences where the ablation rate decreases and a saturation of the parameter can be defined. This effect is more pronounced at the wavelengths of 532 nm and 1064 nm,—for TC-type ceramic at these wavelengths, a well-expressed decrease of the ablation depth is observed as the fluence is increased. The effect could be explained by efficient plasma absorption and shielding of the target. The interaction of the laser radiation with the plasma could take place via two main mechanisms—inverse bremsstrahlung absorption and photoionization [20]. The first type is more efficient for IR radiation due to the $\lambda^3$ dependence of the absorption coefficient. In the VIS and UV ranges, photoionization via absorption by excited states and/or direct ionization is dominant. Furthermore, the application of higher fluences at 1064 nm (due to a higher ablation threshold) may result in air breakdown above the sample. In addition to the efficient plasma absorption, this is an additional channel for ablation rate saturation. It should also be mentioned that the ablation process is accompanied by changes in the material morphology and composition, as shown below, which may alter the efficiency of the laser–matter interaction.

A comparison between the dependences for the two type of ceramics indicates that the ablation rates are similar at 266 nm and 355 nm, and they are higher for the TC ceramic at the wavelengths of 532 nm and 1064 nm.

An extrapolation to zero depth of the data presented in Fig. 1 could be used to estimate the ablation threshold in the different cases. Its value as a function of the irradiation wavelength for the different ceramics is shown in Fig. 2. The estimated values are similar for both ceramics, and a tendency of the ablation threshold increasing with the increase of the laser wavelength is clearly expressed.

Another parameter that may influence the ablation characteristics is the number of the laser pulses applied. It is related to the so-called accumulation effects having to do with changes in the material's optical and thermo-physical properties by the previous pulse. These could be due to modifications of the surface morphology or chemical composition transformations of the material and may significantly

influence the ablation rate. The dependences of the ablation depth on the number of laser pulses for the TC and GP ceramics are given in Fig. 3a and b, respectively. The laser fluences of 6 J/cm$^2$ at 266 nm, 7 J/cm$^2$ at 355 nm, 12 J/cm$^2$ at 532 nm, and 30 J/cm$^2$ at 1064 nm are chosen as values exceeding by a factor of about six as the ablation threshold for the corresponding wavelength. Under the conditions of the most of the cases discussed, a saturation of the ablation rate is not well expressed. The dependences presented in Fig. 3 indicate that two regimes can be defined. When the pulse number is up to 10, a steeper increase of the ablation depth is observed with an average rate of about 2 μm/pulse. This value is similar for all wavelengths and for both types of $Si_3N_4$ ceramics. The second regime can be defined as taking place when the pulse number is above 100. Then, the ablated depth per pulse increases with the increase of the wavelength for both ceramic types. The effect could be related to the increase of the laser fluence used at the different wavelengths and a change in the properties of the material remaining in the ablation area. Furthermore, accumulation effects can also explain the appearance of two regimes whereby the ablation causes changes in the material's composition, morphology, and optical properties. It should be noted that while the ablation depths observed for both ceramics at 1064 nm are clearly different when the number of pulses is raised up to 100, no differences are seen for pulse numbers of 300 and 600. This effect could also be ascribed to accumulation effects. To clarify the changes of the material's properties, SEM analyses of the surface relief were performed. Figure 4a and b presents images of the ablated zone surface of the TC and GP ceramics, respectively, at the different wavelengths used. Structures fabricated by 10 and 600 pulses are shown. The laser fluences applied correspond to those in Fig. 3. Images of the native ceramics surface are also given. The structure of the material below the polished surface is illustrated in the inset in the image of the native GP ceramic. A comparison between the structure of the native materials shows that in the case of TC ceramic, elongated rod-like grains are observed, while these are not present in the GP type. The ablation process changes the ceramic surface morphology—in the case of TC $Si_3N_4$, the specific rod-shaped grains seen in the native material are not present even after just ten pulses at all wavelengths used. Instead, traces of surface melting can be identified. In the cases of using the wavelengths of 532 nm and 1064 nm, the ceramic surface is covered by a well-expressed layer with a morphology completely different compared to the native material. The application of 600 pulses results in the formation of a rough surface structure, which has similar characteristics for all wavelengths. It is expressed by grains with soft edges, which is an indication of melting, and by a fine surface decoration of the entire surface by nanosized particles. Parallel lines could be seen on the surface of the native GP ceramic that

**Fig. 1** Dependences of the ablation depth on the applied laser fluence at the different wavelengths for the two type of ceramics: **a** TC $Si_3N_4$ and **b** GP $Si_3N_4$. The number of laser pulses in all cases is 100. The error bars represent the standard deviation
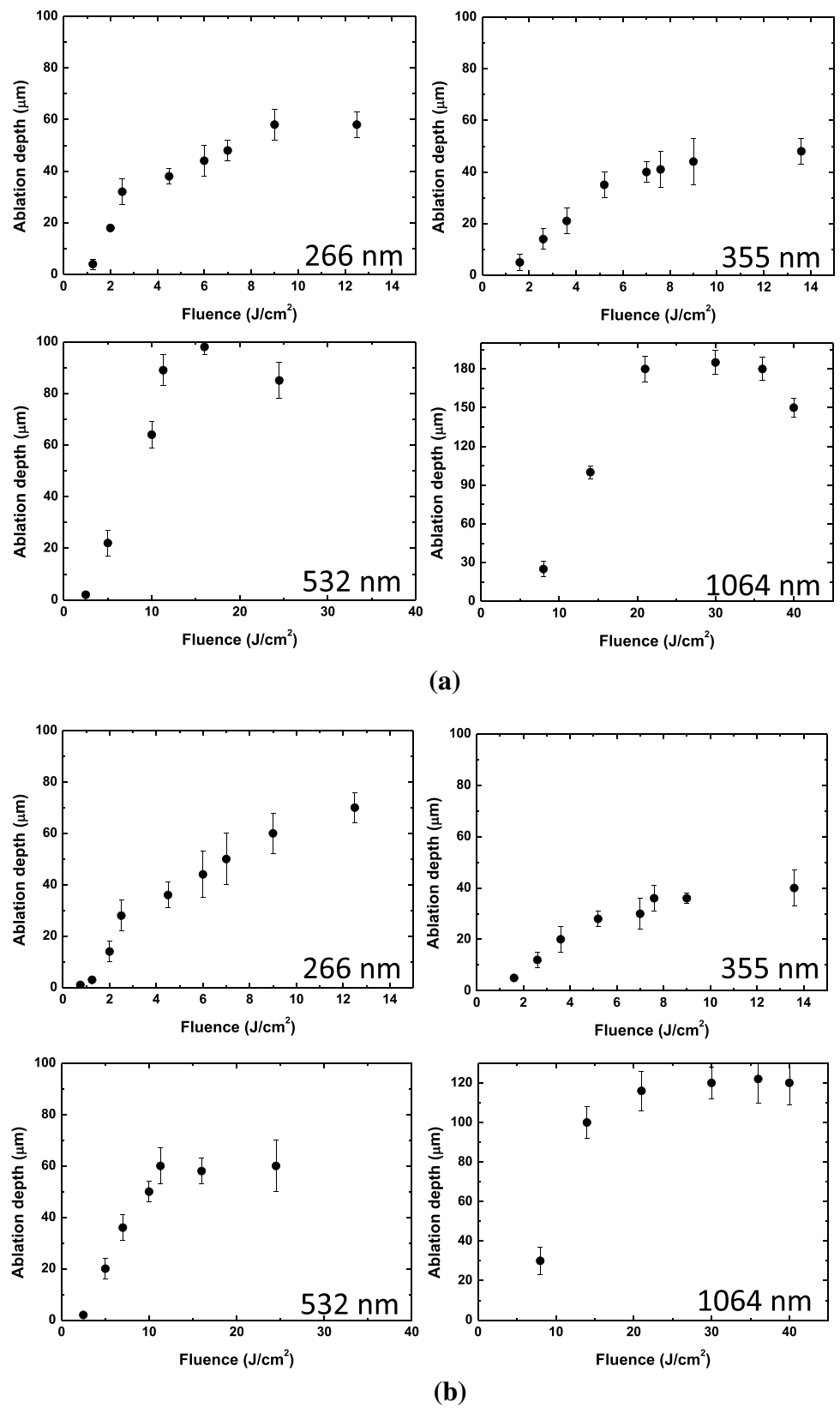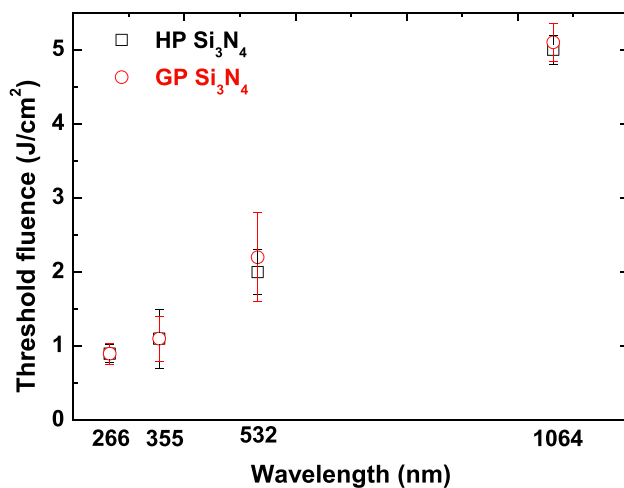
**Fig. 2** Estimated ablation threshold for the two ceramic types at different laser wavelengths. The error bars represent the standard deviation

are related to the mechanical treatment of the material after fabrication (cutting and polishing). The ablation process leads to a fast disappearance of these features—even after just ten laser pulses the surface relief is modified for all wavelengths. The difference in the surface structure depending on the laser wavelength is more expressed at the low pulse number. As seen in Fig. 4b, at 1064 nm and application of ten pulses, the ceramic surface seems to be covered by a flat molten layer. Such a surface structure is not observed for the other wavelengths. Increasing the number of laser pulses applied results in a high similarity of the induced surface structure for the different wavelengths, with the morphology consisting of a porous microstructure. The structure obtained at 266 nm and application of 600 pulses is covered by a fine network of nanoparticles arrayed in well-expressed chains, and micron-sized bumps are also formed. The surface morphology observed for the other wavelengths consists of micron-sized grains with rough edges densely covered by spherical-like nanoparticles and micron- and submicron-sized voids (see the high magnification image presented as inset in Fig. 4b for 1064 nm). It should be mentioned that the effect of the laser fluence change on the surface morphology in the ablated area is somewhat similar with that in the case of changing the number of pulses. At low laser fluences (close to the ablation threshold), the presence of a molten layer can be seen which is better expressed at 532 nm and 1064 nm. Increasing the fluence results in the formation of the surface morphology presented in Fig. 4 for 600 pulses.

The laser-induced surface structuring is also accompanied by changes in the surface material composition. This is demonstrated by Fig. 5, where Raman spectra are presented of the two type of ceramics irradiated at different wavelengths. The laser fluences applied are the same

as indicated in Fig. 3 with the number of pulses being 600. The native materials' spectra are also presented. These indicate that in both cases of ceramics, the $\beta$ phase of Si₃N₄ dominates, and traces of $\alpha$ can also be identified [21, 22]. The laser irradiation changes dramatically the Raman spectra—in all cases presented in Fig. 5 it leads to the appearance of a new peak that is the strongest one. It is located at 519 cm⁻¹ and can be attributed to the appearance of Si [23]. This peak also shows a broadening in the direction of the lower wavenumbers (clearly seen, for example, for GP ceramic irradiated at 266 nm), which can be attributed to the presence of amorphous silicon and/or a microcrystalline fraction. [23, 24]. Further information on the material composition and structure was obtained by XRD analysis. Figure 6a and b shows the spectra for the native and irradiated material for the two ceramic types. The laser processing was carried out at the wavelength of 1064 nm, at 30 J/cm², and application of 600 laser pulses. According to the results of applying the specialized software for phase quantity evaluation, the TC Si₃N₄ ceramic contains about 11% of the α phase and a small amount of SiO₂. In the GP type, the $\alpha$ phase is not recognized and the sample consists of a significant amount of sinoite (Si₂N₂O). Y₂O₃ is also detected, which is usually added to the ceramic to stabilize the material. The Si peak is overlapped by those of Si₃N₄; thus, its presence cannot be identified by this analysis. The effect of laser irradiation consists in a decrease of the peak intensities and the appearance of an amorphous phase (clearly expressed in the case of TC ceramic) as an elevated background in the range 25–50°. This behavior can be explained by the formation of an amorphous surface layer on the ceramic surface. To estimate the composition of the surface layer, XPS analysis was also performed. This method provides information on the material's top surface, so that the signal from the underlying unaffected material is eliminated. Figure 7 presents Si2p XPS spectra for the case of the TC ceramic irradiated at the wavelength of 1064 nm, a fluence of 30 J/cm², and 600 pulses. The convolution of the original spectra shows that mainly a silicon oxide phase is detected after irradiation due to silicon oxidation taking place as a result of a laser-induced decomposition reaction. It should be mentioned that the analysis also points to a significant nitrogen reduction in the irradiated zone. Since the XPS results refer to the surface composition, one can assume that this oxidation expands to some depth where silicon is present (as detected by the Raman spectra). Thus, the combination of the different analyses used here indicates that the surface layer in the ablated area is composed mainly of crystalline/microcrystalline Si and silicon oxide (and possibly surface covered Si). The origin of this composition is the mechanism of the ablation process in Si₃N₄ ceramics, which is realized via decomposition of

**Fig. 3** Dependences of the ablation depth on the number of laser pulses for: **a** TC $Si_3N_4$, and **b** GP $Si_3N_4$ ceramics. The laser fluences at the different wavelengths are: 6 J/cm$^2$ at 266 nm, 7 J/cm$^2$ at 355 nm, 12 J/cm$^2$ at 532 nm, and 30 J/cm$^2$ at 1064 nm. The values are about six times higher than the ablation threshold for the corresponding wavelength. The error bars represent the standard deviation
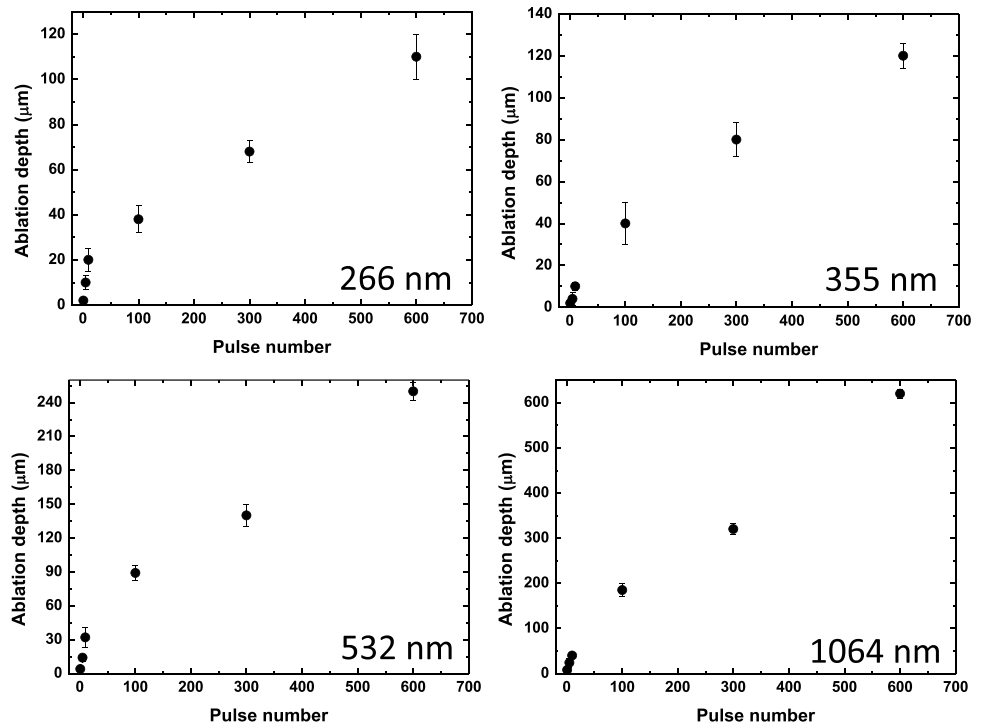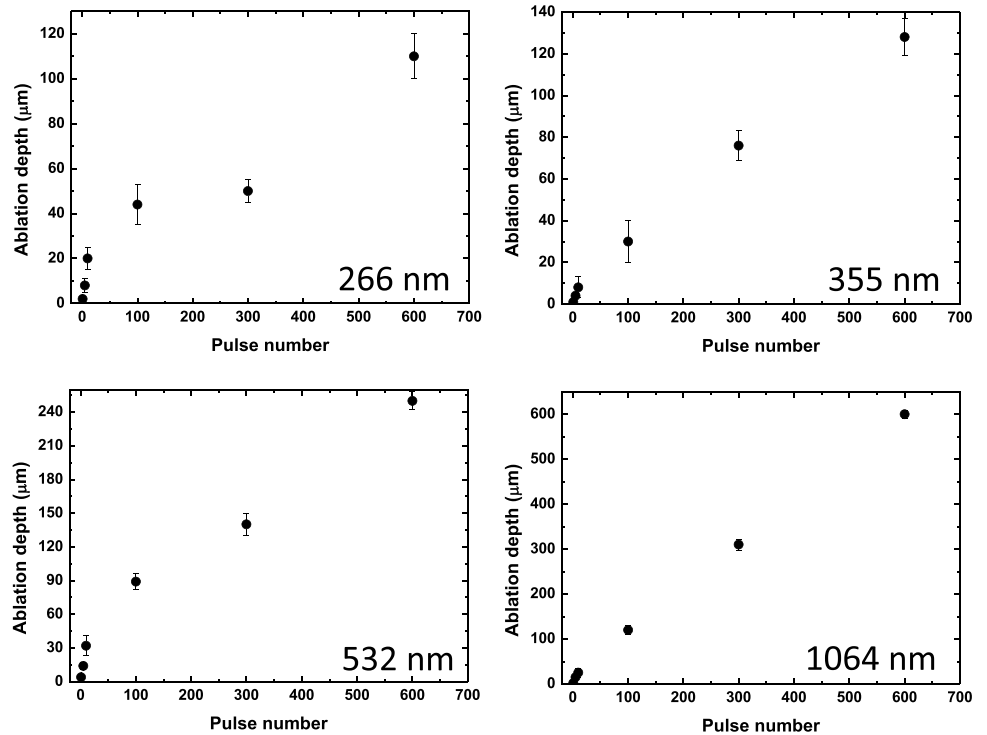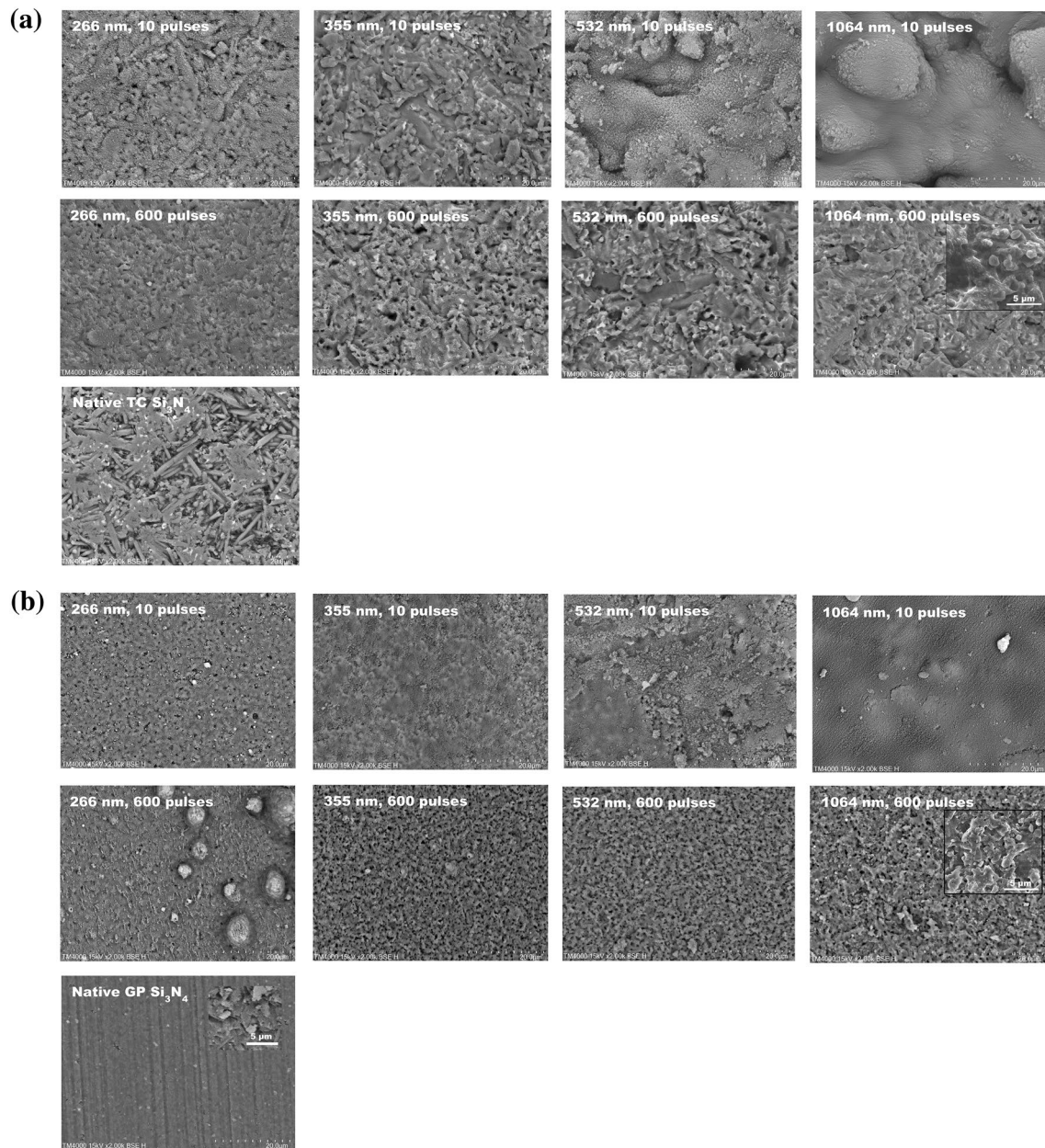
**Fig. 4** SEM images of the surface of the ablated zone in: **a** TC Si₃N₄ and **b** GP Si₃N₄ ceramics at the different wavelengths used. Structures fabricated at 10 and 600 pulses are shown. The laser fluences applied correspond to those in Fig. 3. The width of the images is 60 μm. Images of the surface of the native ceramics are also given. The structure of the material after removing the polished surface is illustrated in the inset in the image of the native GP ceramic

the material—nitrogen is ejected and Si remains on the irradiated surface [2]. At temperature above approximately 1877 °C, a decomposition reaction takes place:

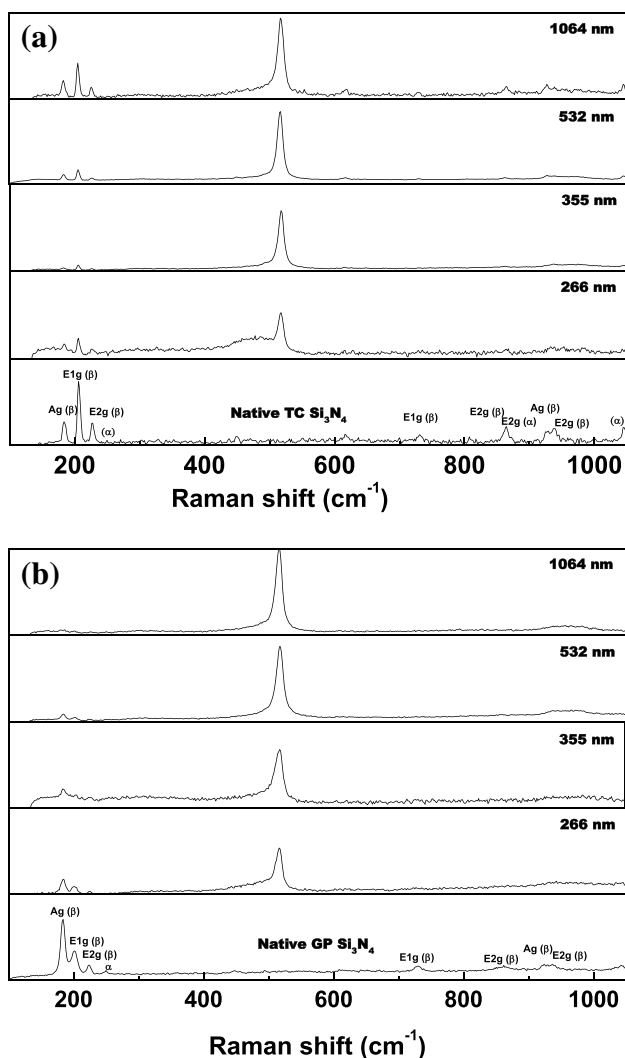$$Si_3N_4 \rightarrow 3Si(liquid) + 2N_2(gas). \tag{1}$$
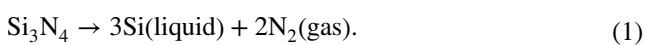
The realization of this reaction is evidenced in this work by the change in the Raman spectra presented above and expressed by the strong Si peak. Since the ablation process occurs in air, the formed silicon is oxidized to a certain depth, as indicated by the strong oxide signal in the XPS spectra.
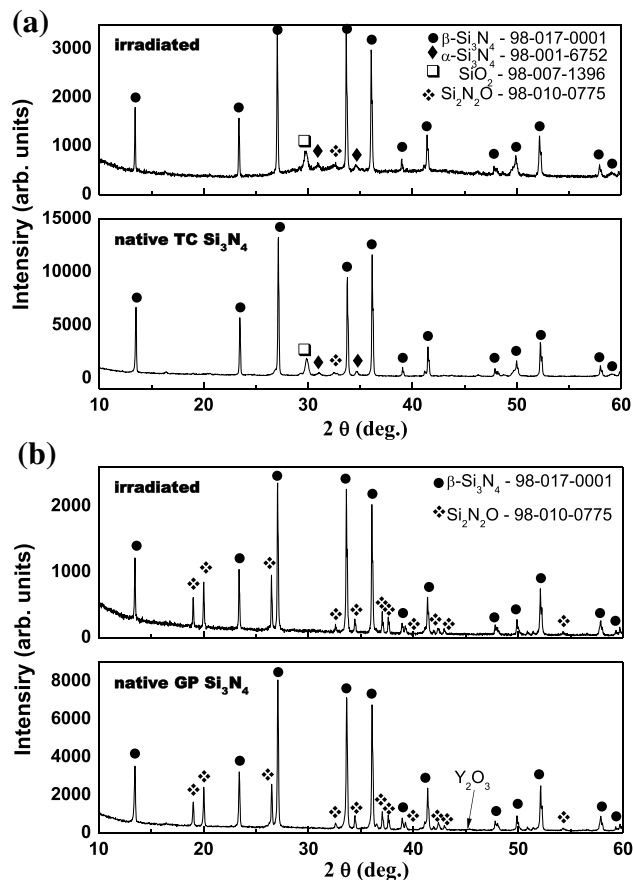
The results presented above demonstrate a similar behavior of the ablation characteristics for the two ceramic types studied when different laser radiation wavelengths are used. This indicates that thermal decomposition is the prime mechanism of ablation in the nanosecond laser pulse regime, independently of the wavelength used. The structures formed on the surface exhibit morphologies that are related to the

**Fig. 6** XRD spectra for the native and irradiated material for: **a** TC $Si_3N_4$ and **b** GP $Si_3N_4$ ceramics. The laser processing is carried out at the wavelength of 1064 nm, fluence of 30 J/cm$^2$, and application of 600 laser pulses. The card numbers used for structure identification are also shown

**Fig. 5** Raman spectra of **a** TC $Si_3N_4$ and **b** GP $Si_3N_4$ ceramics at the different wavelengths used. The laser fluences applied are the same as indicated in Fig. 3. The number of laser pulses is 600. The spectra of the native materials are also presented, and the typical Raman lines of the ceramic are shown. The peaks corresponding to the different $Si_3N_4$ phases are also indicated

ejection of nitrogen and formation of a molten layer. The thickness of the melt formed when irradiation at 1064 nm is used is obviously higher for both ceramics, which could be explained by the lower absorption coefficient of the material at this wavelength compared to the case of UV irradiation. The effect is more pronounced at low number of pulses, which suggests that an accumulation effect begins to dominate at higher number of pulses and the changes in the optical parameters reach a stage where they become similar for all wavelengths used. The initial differences in the optical properties of the ceramic material were analyzed on the basis of the transmission spectra for the TC type of ceramic. In the GP-type case, the samples are thick and no

transmission signal can be detected. The analysis shows that the transmission of TC $Si_3N_4$ at 1064 nm is about twice as high as that at 532 nm and about three times higher than in the case of 355 nm. At 266 nm, the sample allows no transmission. Thus, a thicker surface layer is affected by the laser irradiation at 1064 nm. The same measurement after application of 100 pulses at the wavelength of 1064 nm indicates a decrease of the sample transmission to about 20%.

As is shown in Fig. 4, the changes in the laser parameters strongly influence the surface morphology, so that the effect can be efficiently used for surface structuring of $Si_3N_4$ ceramics.

It should be mentioned that only some results presented in this work can be compared with already published ones due to the significant differences in the processing conditions. However, different authors have used various laser systems, such as continuous-wave (CW) $CO_2$ laser at $\lambda = 10.6$ μm [14], 100 kHz pulsed Nd:YAG at $\lambda = 1064$ nm with a pulse duration of 100 ns [16], 100 kHz Nd:YAG at $\lambda = 532$ nm
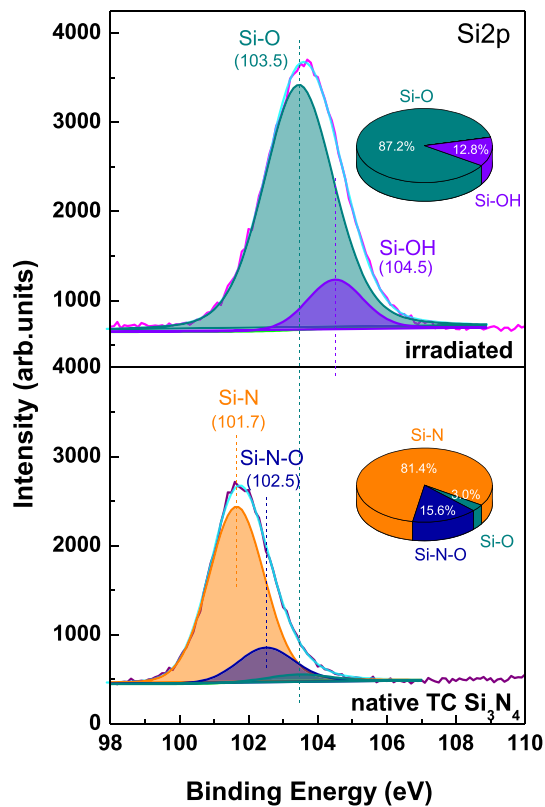
**Fig. 7** Si2p XPS spectra of the material in the ablated zone in TC Si₃N₄ ceramic irradiated atthe wavelength of 1064 nm, fluence of 30 J/cm², and application of 600 pulses.

and a pulse duration of 6 ns [19], and reported that the ablation process is accompanied by material decomposition, efficient silicon oxidation in the ablated zone, and reduction of the N content. It is shown in Ref [17] that CW laser processing in the IR range results in surface melting and a change of the ceramic crystallite shape. This behavior is also observed in the present work for all wavelengths used. It demonstrates that in a wide range of experimental conditions, such as pulse duration from ns to CW and different wavelengths from the UV to the IR, the ablation process in Si₃N₄ ceramic proceeds via material decomposition, formation of silicone oxide, and presence of melt in the affected zone. A reduction of the ablation rate, as presented in Fig. 1, is also reported in Ref [16], in which the authors refer to a change of the coupling efficiency between the laser radiation and modified morphology of the formed ablation hole and the properties of the remaining material. Although the structures presented in our work are characterized by a low aspect ratio (hole depth/hole width), so that multiple reflections from the holes' wall and accumulation of shielding gas phase into the hole could be neglected, changes in the material's morphology and chemical composition are clearly

seen. In contrast to the transition from the $\alpha$ to the $\beta$ phase due to laser irradiation reported in Ref [25], our analyses indicate that ablation is not accompanied by such dynamics. The reason is probably due to the use of a CW laser in Ref. [25] that ensures a heat accumulation significantly higher than that in the case of ns pulses. Since the phase changes are thermally induced, one should expect the efficiency to increase when the heat accumulation is higher.

## 4 Conclusions

In this work, the laser ablation of Si₃N₄ ceramics prepared by tape casting and gas pressure sintering is studied in cases of irradiation by different wavelengths ranging from the UV to the IR emitted by a nanosecond Nd:YAG laser. Despite some quantitative differences, the dependences of the ablation depth on the laser fluence and number of pulses applied exhibit a similar behavior for the two ceramic types and for the different wavelengths used. In all cases, a saturation is observed of the ablation depth increase as the laser fluence is increased. The dependences of the ablation depth on the number of pulses applied at a fixed laser fluence show a linear behavior, while two regimes can be identified. For TC Si₃N₄, the ablation rate (ablation depth per fluence) is higher, especially at 532 nm and 1064 nm. This behavior is observed at application of up to about 100 laser pulses. As the number of pulses is increased, the difference in the ablation rates of the ceramics becomes negligible. Even after the application of a few laser pulses, the laser processing changes significantly the surface morphology, producing mainly surface melting. For the cases of wavelengths of 532 nm and 1064 nm, the ceramic surface is covered by a thick molten layer that completely masks the native ceramic structure, an effect seen for both ceramic types. The combination of the different analytical techniques used to identify this layer's compositions shows that it consists of crystalline and amorphous silicon and silicon oxide. Raising the number of laser pulses results in the formation of a porous surface structure having similar characteristics for all wavelengths and consisting of micron-sized grains densely covered by nanosized particles. The ablation process proceeds via material decomposition—the presence of silicon in the processed area is evidenced by Raman spectroscopy. The study presented can be used in the design of laser-based techniques for Si₃N₄ ceramics processing and surface micro- and nanostructuring and fabrication of Si-containing materials.

# References

1. S.N. Grigoriev, Kh. Hamdy, M.A. Volosova, A.A. Okunkova, S.V. Fedorov, Mat. Design **209**, 109965 (2021)
2. Z. Krstic, V.D. Krstic, J. Mater. Sci. **47**, 535 (2012)
3. V. Onbattuvelli, S. Atre, Mat. Manufact. Proc. **26**, 832 (2011)
4. V. Bharathi, A.R. Anilchandra, Sh.S. Sangam, S. Shreyas, S.B. Shankar, Mat. Today Proc. **46**, 1451 (2021)
5. F.L. Riley, J. Am. Ceram. Soc. **83**, 245 (2000)
6. R.B. Heimann, Ceramics **4**, 208 (2021)
7. B.S. Bal, M.N. Rahaman, Acta Biomat. **8**, 2889 (2012)
8. K.M. Fox, J.R. Hellmann, Int. J. Appl. Ceram. Technol. **5**, 138 (2008)
9. Y. Kobayashi, E. Matsuo, T. Inagaki, T. Ozawa, SAE Paper 910401 (1991)
10. M.H. Bocanegra-Bernal, B. Matovic, Mat. Sci. Engin. A **527**, 1314 (2010)
11. P. Gui-hua, L. Xiang-guo, L. Min, L. Zhen-hua, L. Quian, L. Wen-lan, Scr. Mater. **61**, 347 (2009)
12. Y. Tajima, In:, Silicon Nitride-Scientific and Technological Advances, ed. By I.W. Chen (MRS Symp. Proc. 287, MRS, Pittsburgh, USA, 1993), p. 189
13. F. Riley, S.K. Biswas, F.L. Riley, Mat. Chem. Phys. **67**, 175 (2001)
14. S. Lei, Y.C. Shin, F.P. Incropera, J. Manufact. Sci. Eng. **123**, 639 (2001)
15. A.N. Samant, N.B. Dahotre, J. Manufact. Proc. **12**, 1 (2010)
16. B. Soltani, B. Azarhoushang, A. Zahedi, Opt. Laser Technol. **119**, 105644 (2019)
17. P. Shukla, J. Lawrence, Opt. Laser Technol. **54**, 380 (2013)
18. A.N. Samant, N.B. Dahotre, Adv. Eng. Mater. **11**, 579 (2009)
19. H.-J. Wang, Q. Chen, D.-T. Lin, F. Zuo, Z.-X. Zhao, C.-Y. Wang, H.-T. Lin, Ceram. Intern. **44**, 14925 (2018)
20. N.M. Shaikh, S. Hafeez, B. Rashid, M.A. Baiga, Eur. Phys. J. D **44**, 371 (2007)
21. K. Honda, Sh. Yokoyama, Sh. Tanaka, J. Appl. Phys. **85**, 7380 (1999)
22. N. Wada, S.A. Solin, J. Wong, S. Prochazka, J. Non-Crystalline Solids **43**, 7 (1981)
23. C. Smit, R.A.C.M.M. van Swaaij, H. Donker, A.M.H. Petit, W.M.M. Kessels, M.C.M. van de Sanden, J. Appl. Phys. **94**, 3582 (2003)
24. W.-E. Hong, J.-S. Ro, J. Appl. Phys. **114**, 073511 (2013)
25. P. Shukla, J. Lawrence, Opt. Lasers Eng. **49**, 998 (2011)